Title
RIT1 oncoproteins escape LZTR1-mediated proteolysis.

Journal
Science (New York, N.Y.), 363(6432)

ISSN
0036-8075

Authors
Castel, Pau
Cheng, Alice
Cuevas-Navarro, Antonio
et al.

Publication Date
2019-03-01

DOI
10.1126/science.aav1444

Peer reviewed

Published in final edited form as:

Science. 2019 March 15; 363(6432): 1226–1230. doi:10.1126/science.aav1444.

RIT1 oncoproteins escape LZTR1-mediated proteolysis

Pau Castel[1], **Alice Cheng**[1], **Antonio Cuevas-Navarro**[1], **David B. Everman**[2], **Alex G. Papageorge**[3], **Dhirendra K. Simanshu**[4], **Alexandra Tankka**[5], **Jacqueline Galeas**[1], **Anatoly Urisman**[5], **Frank McCormick**[1,*]

[1]Helen Diller Family Comprehensive Cancer Center, University of California San Francisco, San Francisco, CA, USA.

[2]Greenwood Genetic Center, Greenwood, SC, USA.

[3]National Cancer Institute, National Institutes of Health, Bethesda, MD, USA.

[4]NCI RAS Initiative, Cancer Research Technology Program, Frederick National Laboratory for Cancer Research, Leidos Biomedical Research, Frederick, MD, USA.

[5]Department of Pathology, University of California San Francisco, San Francisco, CA, USA.

Abstract

RIT1 oncoproteins have emerged as an etiologic factor in Noonan syndrome and cancer. Despite the resemblance of RIT1 to other members of the Ras small guanosine triphosphatases (GTPases), mutations affecting RIT1 are not found in the classic hotspots but rather in a region near the switch II domain of the protein. We used an isogenic germline knock-in mouse model to study the effects of RIT1 mutation at the organismal level, which resulted in a phenotype resembling Noonan syndrome. By mass spectrometry, we detected a RIT1 interactor, leucine zipper–like transcription regulator 1 (LZTR1), that acts as an adaptor for protein degradation. Pathogenic mutations affecting either RIT1 or LZTR1 resulted in incomplete degradation of RIT1. This led to RIT1 accumulation and dysregulated growth factor signaling responses. Our results highlight a mechanism of pathogenesis that relies on impaired protein degradation of the Ras GTPase RIT1.

The Ras family of small guanosine triphosphatases (GTPases) is a group of evolutionarily conserved proteins that exhibit high affinity for guanosine di- and triphosphates (GDP and GTP) and activate downstream signaling pathways when bound to GTP (1). GTPase-

*Corresponding author. frank.mccormick@ucsf.edu.

Author contributions: P.C. and F.M. conceived the project, supervised the research, and wrote the manuscript. P.C. prepared the figures. P.C., A.C., A.C.-N., and J.G. performed the experiments. D.B.E. provided patients' samples. A.G.P. performed the GTP loading experiments. D.K.S. performed the LZTR1 modeling. A.T. and A.U. performed MS analysis. All authors commented on and approved the manuscript.

Competing interests: The authors declare no competing interests.

Data and materials availability: The data required to evaluate the conclusions of the paper are described in the main text and supplementary materials. Raw data resulting from MS experiments are available in the MassIVE (MSV000083444) and ProteomeXchange (PXD012718) repositories. Materials can be requested from F.M.

Materials and Methods
Figs. S1 to S8
References (40–49)

SUPPLEMENTARY MATERIALS
www.sciencemag.org/content/363/6432/1226/suppl/DC1

activating proteins (GAPs) or guanine exchange factors enable these GTPases to function as molecular binary switches by modulating their binding to GDP or GTP in response to specific inputs (2). Although NRAS, HRAS, and KRAS are frequently mutated in cancer, RASopathies, a group of developmental disorders, have also been linked to mutations affecting members of the Ras GTPase family (3). For instance, germline or de novo KRAS, NRAS, RIT1, MRAS, and RRAS mutations are found in individuals with Noonan syndrome (NS). These mutations do not occur in the same locations as cancer-causing alleles but rather in secondary locations that render the GTPase "weakly" active (4–8). By contrast, cancer alleles that are refractory to GAP activity are embryonically lethal, restricting their germline transmission (9, 10).

RIT1 is a Ras-related small GTPase that regulates cell survival (11). Mutations in this gene are found in 5 to 9% of patients affected by NS (6, 12) and in other typically *KRAS*- or *NRAS*-driven malignancies, such as lung adenocarcinoma and myeloid leukemias (13, 14). RIT1 mutations do not occur in codons analogous to the classic G^{12}, G^{13}, and Q^{61} alleles, which render the protein resistant to the catalytic activity of GAPs, but rather tend to cluster around the switch II region (Fig. 1A and fig. S1A) (single-letter amino acid abbreviations are defined in the legend to Fig. 1). To study the biological effects of RIT1 mutation, we generated a mouse model containing the disease-associated mutation $M^{90}\rightarrow I$ (M90I) (fig. S1B), which is found in both NS and cancer. Germline expression of the endogenous $RIT1^{M90I}$ allele resulted in a phenotype resembling that of NS in mice (15–17). $RIT1^{M90I/+}$ mice had reduced size and weight compared with wild-type (WT) littermates (Fig. 1B and fig. S1, C and D). Because NS patients are characterized by craniofacial abnormalities, including hypertelorism (increased intraocular distance), wide foreheads, and small chins (18), we assessed these traits in our mice by micro–x-ray computed tomography (μCT). Compared with WT littermates, $RIT1^{M90I}$ mice displayed small skulls, blunt snouts, and hypertelorism (Fig. 1C and fig. S1E). $RIT1^{M90I/+}$ mice had increased heart weight–to–body weight ratios, and by histology, cardiomyocytes appeared enlarged and showed increased proliferation compared with those of WT littermates (Fig. 1D and fig. S1F), consistent with the cardiac defects found in NS patients, including hypertrophic cardiomyopathy (12). Similarly, $RIT1^{M90I/+}$ mice exhibited enlarged spleens, which is consistent with the extramedullary hematopoiesis described in other mouse models of NS (15, 16) (fig. S1G).

To study the molecular events associated with RIT1 mutation, we established mouse embryonic fibroblasts (MEFs) from mice carrying the conditional $RIT1^{M90I/+}$ allele and analyzed mitogen-activated protein kinase (MAPK) activation by measuring the phosphorylation of extracellular signal–regulated kinase (ERK) and MAPK kinase (MEK) and the transcriptional abundance of the downstream readouts *Dusp6* and *Spry2*. Although basal MAPK activation was similar to that in control cells (fig. S2, A and B), upon stimulation with fetal bovine serum (FBS), $RIT1^{M90I/+}$ cells displayed an enhanced response to growth factors (Fig. 1, E and F, and fig. S2, C to E). Moreover, $RIT1^{M90I/+}$ cells and tissues consistently had greater levels of Rit1 protein but similar amounts of *Rit1* mRNA (fig. S2, F to H). To determine whether increased MAPK pathway activation was also observed in other RIT1 alleles, we selected a panel of mutations on the basis of their frequency and distribution in NS and cancer, including the A57G, A77P, E81G, F82L, T83P, Y89H, and M90I variants and the constitutively active artificial allele Q79L, and generated

stable human embryonic kidney 293 (HEK293) cells. Consistent with the MEF results, the results for RIT1 mutants showed an increased and prolonged response to growth factor stimulation (fig. S3A).

HRAS, NRAS, and KRAS proteins are found in the GDP form when purified from cells deprived of growth factors, because of the activity of GAPs, but they exhibit up to 80% GTP loading if they contain oncogenic mutations, as these interfere with GAP catalytic activity (19). To determine whether similar effects occur in RIT1 oncoproteins, we measured the GTP-to-GDP ratio in a panel of cell lines expressing such alleles. WT RIT1 was predominantly bound to GTP in cells depleted of serum, and mutant alleles had either similar or increased GTP loading (fig. S3B). No obvious connection between the GTP binding status of the mutant alleles and their response to growth factors or CRAF interaction was detected (fig. S3, C to F). Therefore, RIT1 oncoproteins are unlikely to be regulated similarly to Ras oncoproteins, by GAP resistance. Moreover, because most oncogenic mutations are located at the switch II region, a domain important for protein-protein interaction (20), we tested whether an alternative interactor could regulate RIT1's activity. By using mass spectrometry (MS) analysis of extracts from cells expressing various tagged versions of RIT1, we identified different peptides for LZTR1 (fig. S4, A and B). LZTR1 is a Kelch and BTB (broad-complex, tramtrack, and bric à brac)-BACK (BTB and C-terminal Kelch) domain–containing protein that acts as a substrate-specific adaptor for the cullin 3 RING E3 ubiquitin ligase (CUL3) (21, 22). To validate our findings, we precipitated glutathione *S*-transferase (GST)–tagged RIT1 from HEK293T cells and showed interaction with endogenous LZTR1 protein (Fig. 2A).

LZTR1 is mutated in a number of NS probands and is mutually exclusive with RIT1 mutations, suggestive of functional redundancy (23, 24). As many members of the Ras GTPase family are highly conserved and share interacting proteins and effectors (1), we tested for LZTR1 interaction with GST-tagged versions of RIT1, RIN, HRAS, NRAS, KRAS, TC21, RRAS, MRAS, RAP1A, RAP1B, and RHEB. In addition to RIT1, endogenous LZTR1 was pulled down only when MRAS was used as bait (Fig. 2B and fig. S5, A and B). We tested the interaction of LZTR1 with RIT1 bound to GDP or GTPγS (a nonhydrolyzable GTP analog). Recombinant RIT1 interacted preferentially with LZTR1 when bound to GDP but not when bound to GTPγS (Fig. 2C). Of the RIT1 oncogenic mutants, none showed detectable binding to endogenous LZTR1, except for the Q79L mutant, which exhibited decreased binding compared with WT RIT1 (Fig. 2D). We also determined the domains of LZTR1 required for RIT1 binding, LZTR1 dimerization, and CUL3 interaction (fig. S5, C to G).

Because LZTR1 selectively binds to CUL3 (fig. S5H) (22) and Rit1 protein abundance was increased in Rit1 M90I isogenic cells, we tested whether LZTR1 expression might lead to RIT1 protein degradation. When LZTR1 was overexpressed in cells, we observed a decrease in RIT1 abundance that could be rescued by the proteasomal inhibitor bortezomib but not the lysosomal inhibitor bafilomycin A (Fig. 3A). Similar results were obtained with the inhibitor MLN4924, which blocks NEDD8 transfer into cullins (25), a necessary step for CUL3 activity, and with the expression of a dominant negative form of CUL3 (26) (Fig. 3B). To determine whether RIT1 proteolysis was the result of ubiquitination, we measured levels

of this posttranslational modification. Because we were unsuccessful at detecting endogenous ubiquitination by standard approaches, we used tandem ubiquitin binding elements (TUBEs), which bind to and preserve mono- and polyubiquitinated chains (27). Upon TUBE coexpression and RIT1 precipitation, we detected RIT1 ubiquitination in an LZTR1-dependent manner. Ubiquitination was recognizable as a ladder of bands that were immunoreactive to the K48-specific, but not the K63-specific, ubiquitin antibody, a hallmark of proteasome-targeted degradation (Fig. 3C). We used MS and identified peptides for residues K187 and K135 containing the diGly remnant, a modification that indicates ubiquitination, only when TUBEs and LZTR1 were present (Fig. 3D and fig. S6). Consistent with the identification of these ubiquitination sites, K135R and K187R double mutation abolished RIT1 degradation (fig. S7A). We tested whether RIT1 mutations that abolish LZTR1 interaction also prevent proteolysis. The coexpression of LZTR1 led to RIT1 degradation, but not when RIT1 oncogenic mutations were present (Fig. 3E). Consistent with this observation, a decrease in RIT1 ubiquitination was observed in the mutants (fig. S7, B and C).

LZTR1 is mutated in NS, as well as cancer and schwannomatosis (22, 23, 24, 28). In the case of NS, mutations in affected families occur with a recessive pattern and are loss-of-function mutations (24). Point mutations described previously are grouped mostly at the Kelch repeats, six-bladed β-propeller motifs required for substrate recognition (Fig. 3F and fig. S7, D to F). We tested a panel of LZTR1 mutations described in NS families and found that almost all of the mutants failed to promote RIT1 degradation (Fig. 3G). In some cases, this was the result of decreased interaction with RIT1 (fig. S7G).

Because LZTR1 mutations are loss of function, we knocked out *LZTR1* in HEK293T and HeLa cells and demonstrated that RIT1 protein abundance was increased (fig. S8, A and B). *Lztr1* knockout (KO) mice are not viable 29, 30), but we generated MEFs from embryonic day 13.5 embryos, which do not display any appreciable phenotype (fig. S8C). *Lztr1* KO MEFs exhibited increased amounts of Rit1 protein, but not Kras or Hras, compared with those from WT and heterozygous littermates (Fig. 4A and fig. S8, D and E). Additionally, *Lztr1* KO MEFs revealed an enhanced response to growth factors in comparison with MEFs derived from WT littermates (Fig. 4, B and C, and fig. S8, F to H). In HEK293T *LZTR1* KO cells, we also observed an increased MAPK response to serum stimulation, a phenotype that was rescued upon RIT1 KO (fig. S8, I and J). Both of our cellular models corroborate LZTR1 regulation of RIT1 protein stability, so we decided to validate our findings in fibroblasts derived from an NS family carrying recessive alleles in LZTR1. We established primary skin fibroblasts from a father and a mother that contained an LZTR1 R210X mutation (where X represents a stop codon) and a c.2220–17C→A mutation, respectively, and four children that had both affected alleles. The four children with biallelic *LZTR1* mutations had a prominent NS phenotype, although the parents were asymptomatic (24). RIT1 was more abundant in the children than in the unaffected parents and two unrelated controls (Fig. 4D and fig. S8K).

Mutations in Cul3-adaptor proteins such as LZTR1 are responsible for human pathogenesis, including KLHL7 in retinitis pigmentosa (31) and Crisponi/cold-induced sweating syndrome

(32), KLHL3 in pseudohypoaldosteronism (33), KLHL24 in epidermolysis bullosa (34), KLHL40 in nemaline myopathy (35), and KLHL16 in giant axonal neuropathy (36).

A direct role for LZTR1 mutations in NS has been well established, and in accordance with this, mutations lead to enhanced RAS-MAPK signaling (37). However, the precise role of LZTR1 has been unclear. Recent reports suggest a direct interaction with LZTR1 and RAF1-PP1CB complexes (38) or with RAS proteins that then undergo ubiquitination (30, 39). We have not been able to confirm these interactions; rather, we propose a biological relation between LZTR1 and the RAS family member RIT1. Under normal conditions, LZTR1 promotes RIT1 proteolysis through CUL3-mediated proteasomal degradation. Pathogenic mutations affecting RIT1 or LZTR1 lead to RIT1 stabilization and contribute to hyperactivation of MAPK signaling (fig. S8L). This mechanistic insight may open therapeutic strategies for patients carrying *LZTR1* mutations and demonstrates the regulation of Ras GTPases by proteolysis.

Supplementary Material

Refer to Web version on PubMed Central for supplementary material.

ACKNOWLEDGMENTS

We thank J. Johnston and L. Biesecker (NIH) and K. Rauen (UC Davis) for sharing preliminary results and providing advice and members of the McCormick lab for their input. We also thank T. Huynh and Y. Seo for their expertise and technical support with μCT analysis.

Funding: This work was supported by a grant from the NCI (1R35CA197709-01 to F.M.). P.C. is a fellow of the Jane Coffin Childs Memorial Fund for Medical Research. A.C.-N. is a fellow of the NSF Graduate Research Fellowship Program. We thank the UCSF Mass Spectrometry Facility and A. L. Burlingame for providing MS instrumentation support for this project (funded by the NIH grants P41GM103481 and S10OD016229).

REFERENCES AND NOTES

1. Simanshu DK, Nissley DV, McCormick F, Cell 170, 17–33 (2017). [PubMed: 28666118]
2. Bos JL, Rehmann H, Wittinghofer A, Cell 129, 865–877 (2007). [PubMed: 17540168]
3. Tidyman WE, Rauen KA, Hum. Mol. Genet 25, R123–R132 (2016). [PubMed: 27412009]
4. Schubbert S et al., Nat. Genet 38, 331–336 (2006). [PubMed: 16474405]
5. Cirstea IC et al., Nat. Genet 42, 27–29 (2010). [PubMed: 19966803]
6. Aoki Y et al., Am. J. Hum. Genet 93, 173–180 (2013). [PubMed: 23791108]
7. Higgins EM et al., JCI Insight 2, e91225 (2017). [PubMed: 28289718]
8. Flex E et al., Hum. Mol. Genet 23, 4315–4327 (2014). [PubMed: 24705357]
9. Tuveson DA et al., Cancer Cell 5, 375–387 (2004). [PubMed: 15093544]
10. Chen X et al., Proc. Natl. Acad. Sci. U.S.A. 106, 7979–7984 (2009). [PubMed: 19416908]
11. Shi GX, Cai W, Andres DA, Cell. Signalling 25, 2060–2068 (2013). [PubMed: 23770287]
12. Yaoita M et al., Hum. Genet 135, 209–222 (2016). [PubMed: 26714497]
13. Berger AH et al., Oncogene 33, 4418–4423 (2014). [PubMed: 24469055]
14. Gómez-Seguí I et al., Leukemia 27, 1943–1946 (2013). [PubMed: 23765226]
15. Araki T et al., Nat. Med 10, 849–857 (2004). [PubMed: 15273746]
16. Hernández-Porras I et al., Proc. Natl. Acad. Sci. U.S.A. 111, 16395–16400 (2014). [PubMed: 25359213]
17. Wu X et al., J. Clin. Invest 121, 1009–1025 (2011). [PubMed: 21339642]

18. Roberts AE, Allanson JE, Tartaglia M, Gelb BD, Lancet 381, 333–342 (2013). [PubMed: 23312968]
19. Trahey M, McCormick F, Science 238, 542–545 (1987). [PubMed: 2821624]
20. Quilliam LA et al., J. Biol. Chem 271, 11076–11082 (1996). [PubMed: 8626650]
21. Stogios PJ, Downs GS, Jauhal JJS, Nandra SK, Privé GG, Genome Biol. 6, R82 (2005). [PubMed: 16207353]
22. Frattini V et al., Nat. Genet 45, 1141–1149 (2013). [PubMed: 23917401]
23. Yamamoto GL et al., J. Med. Genet 52, 413–421 (2015). [PubMed: 25795793]
24. Johnston JJ et al., Genet. Med 20, 1175–1185 (2018). [PubMed: 29469822]
25. Soucy TA et al., Nature 458, 732–736 (2009). [PubMed: 19360080]
26. Jin J, Ang XL, Shirogane T, Wade Harper J, Methods Enzymol. 399, 287–309 (2005). [PubMed: 16338364]
27. Yoshida Y et al., Proc. Natl. Acad. Sci. U.S.A. 112, 4630–4635 (2015). [PubMed: 25827227]
28. Piotrowski A et al., Nat. Genet 46, 182–187 (2014). [PubMed: 24362817]
29. Dickinson ME et al., Nature 537, 508–514 (2016). [PubMed: 27626380]
30. Steklov M et al., Science 362, 1177–1182 (2018). [PubMed: 30442762]
31. Friedman JS et al., Am. J. Hum. Genet 84, 792–800 (2009). [PubMed: 19520207]
32. Angius A et al., Am. J. Hum. Genet 99, 236–245 (2016). [PubMed: 27392078]
33. Louis-Dit-Picard H et al., Nat. Genet 44, 456–460 (2012). [PubMed: 22406640]
34. Lin Z et al., Nat. Genet 48, 1508–1516 (2016). [PubMed: 27798626]
35. Ravenscroft G et al., Am. J. Hum. Genet 93, 6–18 (2013). [PubMed: 23746549]
36. Bomont P et al., Nat. Genet 26, 370–374 (2000). [PubMed: 11062483]
37. Motta M et al., Hum. Mol. Genet 10.1093/hmg/ddy412 (2018).
38. Umeki I et al., Hum. Genet 138, 21–35 (2019). [PubMed: 30368668]
39. Bigenzahn JW et al., Science 362, 1171–1177 (2018). [PubMed: 30442766]

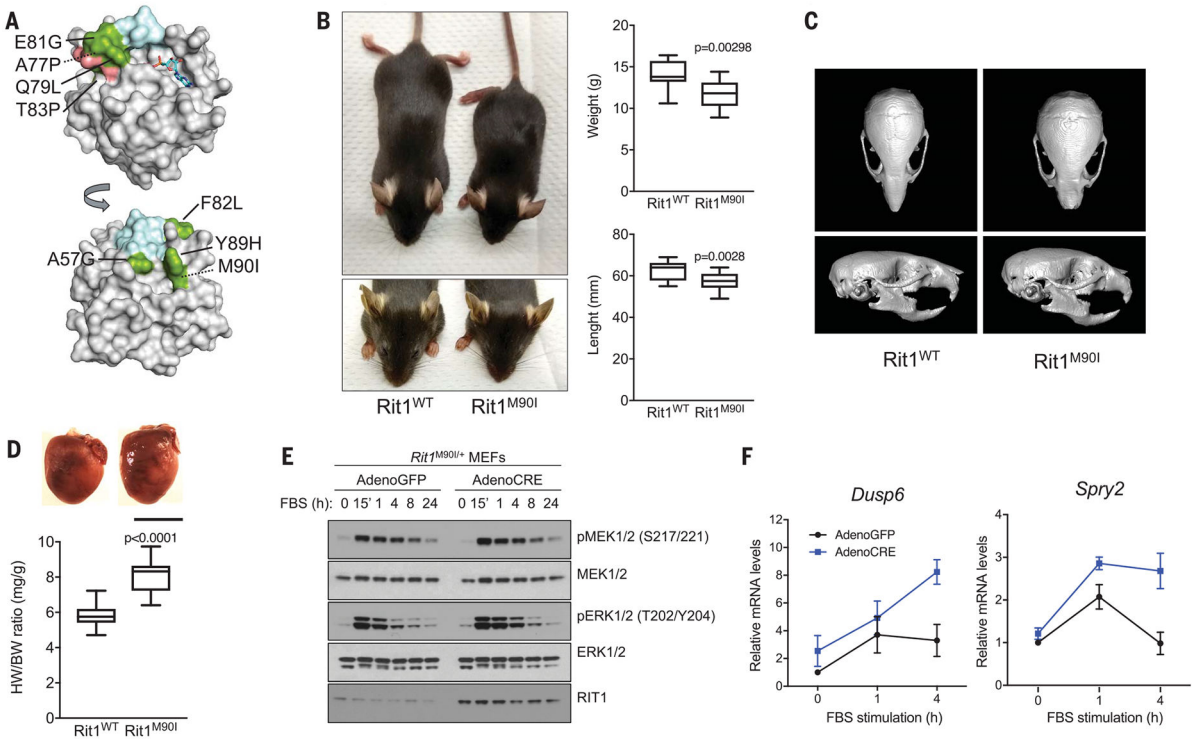

Fig. 1. RIT1 mutants in NS and growth factor response.

(**A**) RIT1 structure model on the basis of the RIT1 GDP crystal structure [Protein Data Bank (PDB) code 4KLZ]. Switches I and II are highlighted in blue and pink, respectively. Mutations are highlighted in green and labeled. Dotted lines represent buried residues. Single-letter abbreviations for the amino acid residues are as follows: A, Ala; C, Cys; D, Asp; E, Glu; F, Phe; G, Gly; H, His; I, Ile; K, Lys; L, Leu; M, Met; N, Asn; P, Pro; Q, Gln; R, Arg; S, Ser; T, Thr; V, Val; W, Trp; and Y, Tyr. (**B**) Representative image of the gross morphological features of Rit1 WT and M90I male mice. Morphometric values are plotted as weight and length at 4 weeks of age. WT, $n = 19$ mice; M90I, $n = 17$ mice. The P values were calculated by using the Mann-Whitney test. (**C**) μCT imaging of Rit1 WT and M90I mouse skulls (male). (**D**) Morphology of the hearts isolated at 8 weeks of age from Rit1 WT and M90I male littermates. Scale bar, 500 μm. The ratio of heart weight (HW) (in milligrams) to body weight (BW) (in grams) for Rit1 WT ($n = 20$) and M90I ($n = 10$) littermates is indicated. The P value was calculated by using the Mann-Whitney test. (**E**) Western blot analysis of primary conditional $Rit1^{M90I/+}$ MEFs infected with adenovirus expressing either green fluorescent protein (GFP) or CRE recombinase and stimulated with FBS at the indicated time points ($n = 3$ samples). (**F**) Quantitative polymerase chain reaction (qPCR) analysis for *Dusp6* and *Spry2* mRNAs from MEFs in (E) ($n = 3$ samples). Error bars in (F) indicate SEM.

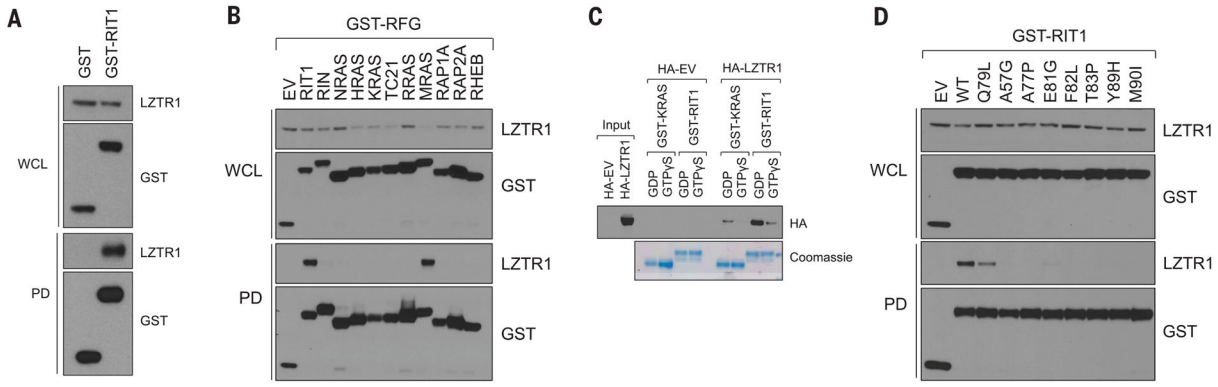

Fig. 2. RIT1 interacts with LZTR1.

(**A**) Proteins precipitated from extracts of HEK293T cells transiently transfected with GST and a GST-RIT1 construct were immunoblotted for endogenous LZTR1. WCL, whole-cell lysate; PD, pulldown. (**B**) Proteins precipitated from extracts of HEK293T cells transiently transfected with a panel of GST-tagged Ras-related GTPases were probed for endogenous LZTR1. EV, empty vector. (**C**) Recombinant GST-RIT1 and KRAS proteins loaded with either GDP or GTPγS were incubated with hemagglutinin (HA)–tagged LZTR1 protein expressed ectopically from HEK293T cell extracts. (**D**) Proteins precipitated from extracts of HEK293T cells transiently transfected with a panel of GST-tagged RIT1 mutants and immunoblotted for endogenous LZTR1.

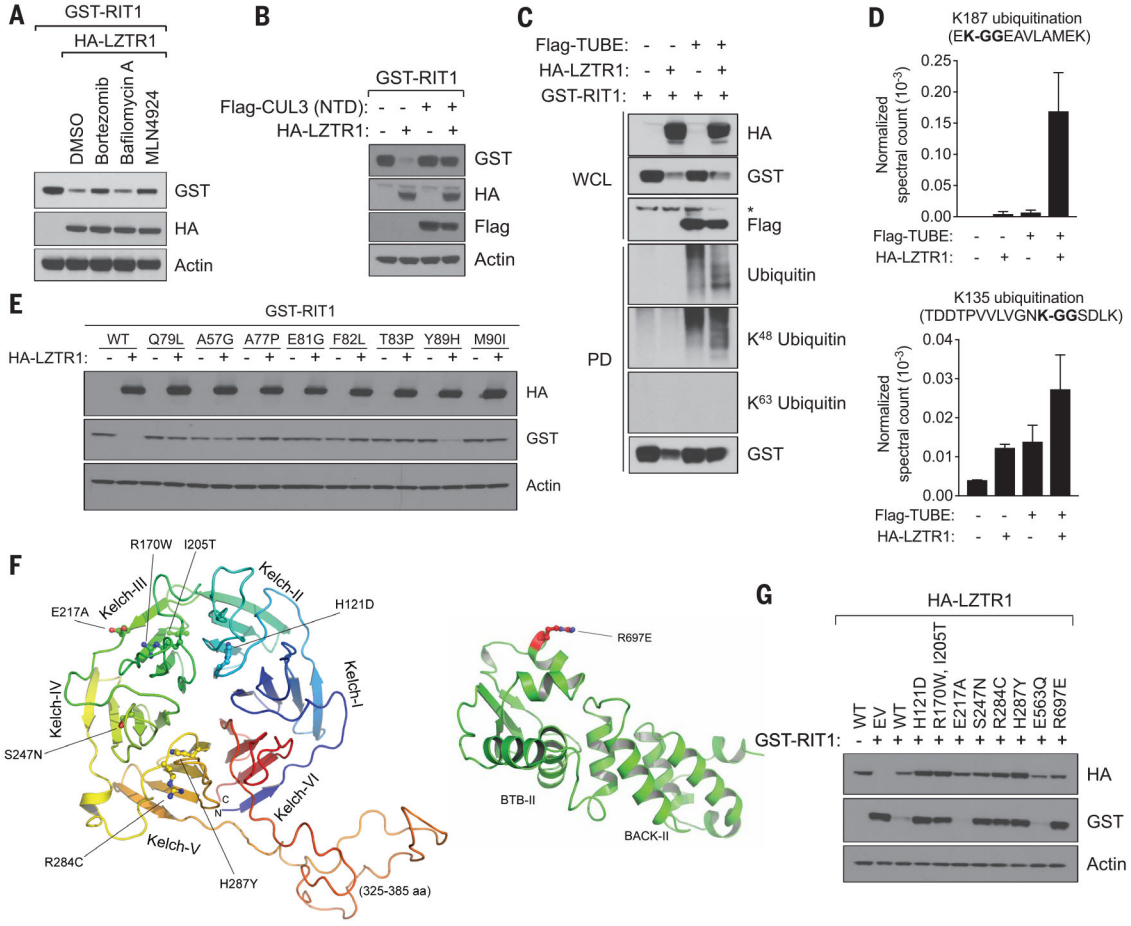

Fig. 3. Degradation of RIT1 by LZTR1.

(**A**) Immunoblot analysis of HEK293T cells overexpressing GST-tagged RIT1 and HA-LZTR1 and treated with bortezomib (100 nM), bafilomycin A (100 nM), or MLN4924 (1 μM) for 8 hours. DMSO, dimethyl sulfoxide. (**B**) Immunoblot analysis of HEK293T cells overexpressing GST-tagged RIT1 and HA-LZTR1 in the presence or absence of the dominant negative cullin 3 N-terminal domain (NTD) (amino acids 1 to 418). (**C**) Ubiquitination of GST-tagged RIT1 from HEK293T cells transfected as indicated with HA-LZTR1 and Flag-TUBE constructs. GST-associated proteins were used to detect RIT1 ubiquitination with specific antibodies. (**D**) MS quantification of diGly-containing peptides in RIT1 in proteins isolated from the experiment in (C). Error bars indicate SEM. (**E**) Immunoblot of HEK293T cells transfected with a panel of GST-tagged RIT1 mutants in the presence of an empty vector or HA-LZTR1. (**F**) Homology-based model of the Kelch (left) (PDB code 5A11) and BTB-BACK2 (right) (PDB code 4J8Z) domains of LZTR1 indicating the locations of the mutations found in NS. aa, amino acids. (**G**) Immunoblot of HEK293Tcells transfected with GST-RIT1 and a panel of HA-tagged LZTR1 mutants described in NS patients.

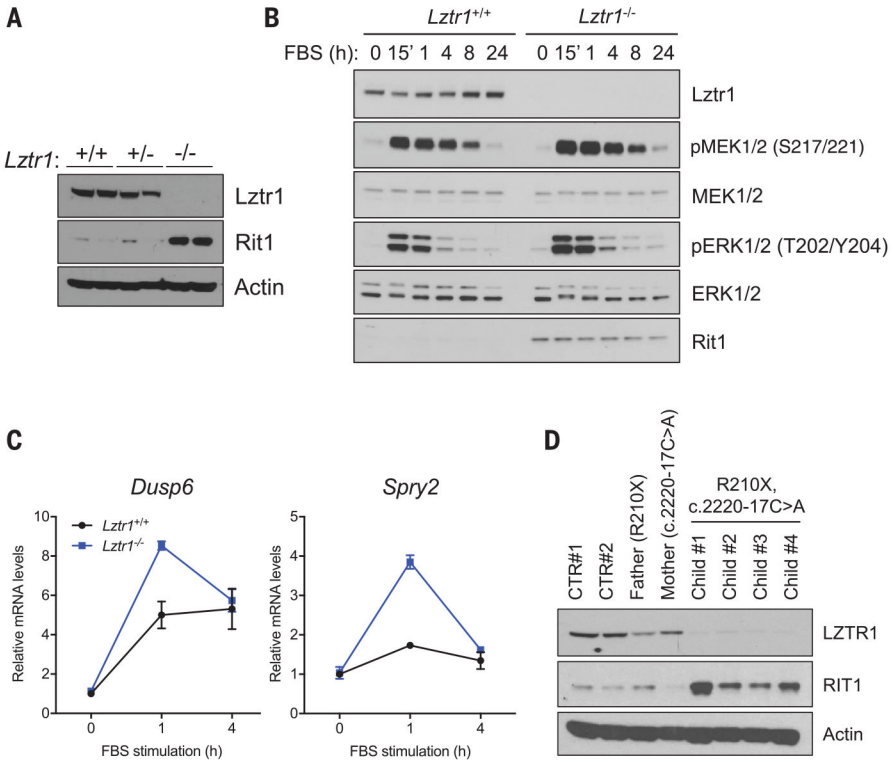

Fig. 4. LZTR1 deletion results in RIT1 stabilization.

(**A**) Immunoblot showing the abundance of Rit1 protein in *Lztr1* WT (+/+), heterozygous (+/−), and KO (−/−) MEFs. Each lane represents an independent cell line derived from a single embryo (two lines per genotype). (**B**) Immunoblot of phosphorylated ERK and MEK in lysates from *Lztr1* WT and KO MEFs deprived of serum and then stimulated with 10% FBS at the indicated time points ($n = 3$ samples). (**C**) qPCR analysis for the indicated transcripts in *Lztr1* WT and KO MEFs deprived of serum overnight and stimulated with 10% FBS for 1 hour ($n = 3$ samples). Error bars indicate SEM. (**D**) Effect of pathogenic LZTR1 R210X and c.2220–17C→A mutations on RIT1 stability in an NS family as shown by immunoblotting. CTR, control.